Measurement 166 (2020) 108214

Contents lists available at ScienceDirect

Measurement

journal homepage: www.elsevier.com/locate/measurement

Development and laboratory evaluation of a self-monitoring polymer geobelts

Jiong Zhang*, Rui She, Shuang Xia, Zhaoxia Dai, Nian Hu, Xinzhuang Cui, Ruonan Han, Ruiping Ming, Guodong Ma

Shandong University, 17922 Jingshi Road, Jinan, China

ARTICLE INFO

Article history:
Received 12 February 2020
Received in revised form 24 May 2020
Accepted 7 July 2020
Available online 15 July 2020

Keywords:
Self-monitoring polymer Geobelts
Resistance
Stress
Strain
Tensoresistivity

ABSTRACT

Due to the rise of smart city construction in recent years, there is a growing demand for materials that can both improve the mechanical properties of structures and carry out health monitoring and risk warning. In this paper, a self-monitoring polymer geobelt manufactured by 3D printing technology is proposed, which can embed conductive ABS material directly into non-conductive PLA material as conductive wire. This integrated resistance geobelt solves the problem of sensor contact to the outside of the grid and water which is easy to fall off and the test results are inaccurate. In this study, a series of tests were performed to study the development and laboratory evaluation of a tensoresistivity geobelts and conclusions were drawn as follows: The self-monitoring polymer geobelt made with PLA and conductive ABS showed good self-perception characteristics and recoverability, and the more the number of longitudinal layout of internal conductive wires, the more accurate the results showed. The relationship between resistance and tensile stress after normalized at ends of the geobelt can be fitted by parabola $f = A + Br + Cr^2$, and the strain of smart geobelt ranges from 2.1 to 10%.

1. Introduction

Due to the rise of smart city construction in recent years, there is a growing demand for materials that can both improve the mechanical properties of structures and carry out health monitoring and risk warning. Geogrid is a kind of main geosynthetical material, which is often used as reinforcement of reinforced earth structures or composite materials. By integrating with a series of sensors like a stress meter or fiber optic, the geosynthetics are capable of sensing strains, temperature or other parameters when used for reinforcement [1].

Over the past two decades, adhered electrical resistance strain gauges had been widely used as sensing components when integrated with geogrids, and diverse methods for installing strain gauges on geogrids were investigated [2–5]. However, the strain gauges adhered on geogrids were susceptible to fall off, and the gauges might be affected by moisture or electromagnetic interference when being used in harsh environments, which provided unreliable strain measurement results [6].

Scholars conducted an in-depth study regarding development and application of smart geogrids embedded with fiber optic sensors [7–10]. Geogrids being knitted only are unavailable for application since their low stiffness. Also, their junctions are susceptible to slip, which may cause the embedded fiber optic to be stripped from geogrids [6]. The maximum strain of fiber optic is about one thousandth, and its application in civil engineering with large deformation is limited, e.g. the deformation measurement of embankment or side slope.

Polymer composites filled with fibers, particulates or metals can generally enhance the properties of the host polymer such as mechanical strength, stiffness, hardness, abrasion resistance and heat deflection temperature while reducing shrinkage and creep [11]. Recently, Cui et al. [12–14] have studied the tensoresistivity properties of geogrids doped with conductive polymers. These geogrids not only realize reinforcement, but also realize self-monitoring function. More recent applications of polymer composites include structural self-sensing, electromagnetic interference shielding, and thermal interfacing [15–17].

Hatami et al. [18–33] developed tensoresistive coating composites by modifying their CB concentrations in order to develop sensorenabled geogrids. They reported a study on the strain sensitivity response of polyvinylchloride/carbon black (PVC/CB) composites' electrical conductivity (tensoresistivity) subjected to cyclic tensile loading. Results showed that the conductive network in the coating specimens filled with the higher-structure CB experienced less

* Corresponding author.
E-mail addresses: jiongzhang@sdu.edu.cn (J. Zhang), cuixz@sdu.edu.cn (X. Cui).

https://doi.org/10.1016/j.measurement.2020.108214
0263-2241/

damage upon cyclic deformation and showed a greater degree of recoverability in their tensoresistivity response. Then conducted to develop a new generation of geosynthetic materials based on the tensoresistivity of polymers filled with electrically conducting particles. [31]

Cui et al. [12–14] developed a new smart geosynthetic named sensor-enabled geobelt (SEGB). The SEGB of high-density polyethylene (HDPE) filled with carbon black (CB) were fabricated by both the industry and the laboratory. Hot pyrocondensation pipes (HPP) were used to protect the SEGB against the influence of water. However, adding a layer of shell to the geogrid increases the difficulty of making geogrid and has the risk of failure [14].

D'Alessandro A et al. [34] presented a systematic investigation on various procedures for fabricating carbon-nanotube-cement pastes, mortars and concretes. They used chemical dispersants and different mixing strategies to achieve dispersion of nanotubes in water, while quality of nanotubes' dispersion is assessed by measuring the rate of nanotube separation and by SEM inspections. Avilés et al. [35] introduced the carbon-filled polymer composites by scholars since 2004. They found that the majority of published works were on epoxy composites filled with MWCNTs, and substantial work had also been published using a variety of thermoplastic and elastomeric matrices such as thermoplastic-polyurethanes (TPUs) and polydimethylsiloxane (PDMS). Poudel A et al. [36] addressed the problem of dispersion of nano-additives in thermoplastic elastomers using continuous processing techniques. Supercritical fluid (SCF) assisted extrusion was utilised to develop elastic, isotropic and electrically superior materials, which contain elastomeric microphases of Poly and tensile strain conditions for smart applications.

To the best of the authors' knowledge, there are no other effective methods to resolve the surrounding moisture influence on the conductivity of polymer composites geogrid in the previous studies, which will limit the application of them in engineering. In this paper, an integrated tensoresistive geobelt manufactured by 3D printing technology is proposed, which can embed conductive ABS material directly into non-conductive PLA material as conductive wire. The stress and deformation of geogrid are reflected according to the principle that conductive wire resistance increases with the decrease of cross-sectional area. This integrated resistance geobelt solves the problem of sensor contact with the outside water which may cause the failure and inaccurate of test results. 3D printing technology was used for preparing the specimens, there is no need for molds in the preparing of such geobelts, as long as geometric models are built in the computer can be mass produced, which increases the repeatability and reduces the time cost.

2. Materials

Experimental specimens made by 3D printing technology in this paper. The 3D printing materials include polylactic acid (PLA) and Acrylonitrile Butadiene Styrene (ABS). The physical properties of the two materials are shown in Table 1.

Conductive materials in specimens ware made of carbon fiber powder with a diameter of 7 μm and a length of around 10 μm as the conductive filler, PLA and ABS powder as the matrix, PBS powder as the toughening agent. The conductive composite particles were prepared by mixing and granulating with a twin screw extruder after mixing by a banbury mixer. The PLA/ABS conductive 3D printing consumables with a diameter of 1.75 mm were made by extruding these particles again through a single-screw or double-screw extruder. The specific steps are as follows: first, PLA or ABS and PBS were crushed into powder by hammer crusher respectively, and the powder particle size was controlled at 40–200 mesh. Then the raw material was weighed according to the following percentage, the carbon fiber powder was 5%, the PLA or ABS powder was 75%, and PBS powder was 20%. The raw materials are mixed in the banbury mixer for 60–120 min under 30–100 °C. Then, the composite material was prepared by drying it in a constant temperature drying oven for 4–12 h at a temperature of 60–100 °C. After that, the composite materials were blended and granulated with a twin-screw extruder, and the composite conductive particles with a diameter of 1–3.5 mm and a length of 46 mm were obtained. In the extrusion process, the screw speed is controlled at 15–30 r/min, the temperature is controlled at 175–225 °C, the inlet and outlet pressure is 35–60 MPa. Finally, the composite conductive particles are extruded again by a single or a twin-screw extruder and collected by the winding machine after cooling. PLA or ABS conductive 3D printing consumables can be prepared by adjusting the traction force and speed to control the diameter of extrusions to 1.75 mm. The conductive 3D printing consumable produced by this preparation process has good stability, electrical conductivity and good mechanical properties. The production process is shown in Fig. 1.

Table 1
The physical properties of the two materials.

Materials	Density (kg/m^3)	Tensile strength (MPa)	Elongation at break (%)
PLA	1.24	50 ± 1.3	2.0 ± 0.4
ABS	1.04	30 ± 1.3	3.6

As shown in Fig. 2 that the carbon fiber powder is evenly distributed in the 3D printing consumables.

The resistance of conductive material per unit length is measured and its resistivity is calculated according to the following formula.

$$\rho_s = R_s \frac{S}{l} \tag{2-1}$$

where ρs is the resistivity; Rs is the resistance; S is the cross-sectional area of conductive material; and l is the conductive material length.

The resistivity of conductive PLA material is 6.73 Ω·m, and that of ABS material is 28.85 Ω·m.

Dual-nozzle 3D printer is used to print geobelt specimens. One extruded non-conductive material is used as the main part of geobelt specimens, and the other extruded conductive material is used as the sensitive element embedded in geobelt to reflect resistance value. 3d models of geobelt samples were built, and then the models were imported into the 3D printer for sample production.

All the 3D printing consumables used in the experiment are 1.75 mm in diameter. The printing accuracy is 0.4 mm, the printing speed is 45 mm/s, and the filling density is 100%. The temperature of the first printing head is 210 °C for extruding PLA consumables, and the second printing head is 230 °C for extruding ABS consumables.

3. Test

The PLA (P) and ABS (A) selected in this paper are host polymer for geobelt specimens, and the conductive PLA (CP) and ABS (CA) are selected for filling conductive materials. In order to achieve the best effect of material combination and distribution of conductive wire, a preliminary experiment was carried out. After determining the experimental material and the shape of the conductive wire, the tensile test with different amounts of conductive wire, slow loading deformation test and repeatability test were carried out for the geobelt specimens. Resistance changes of the

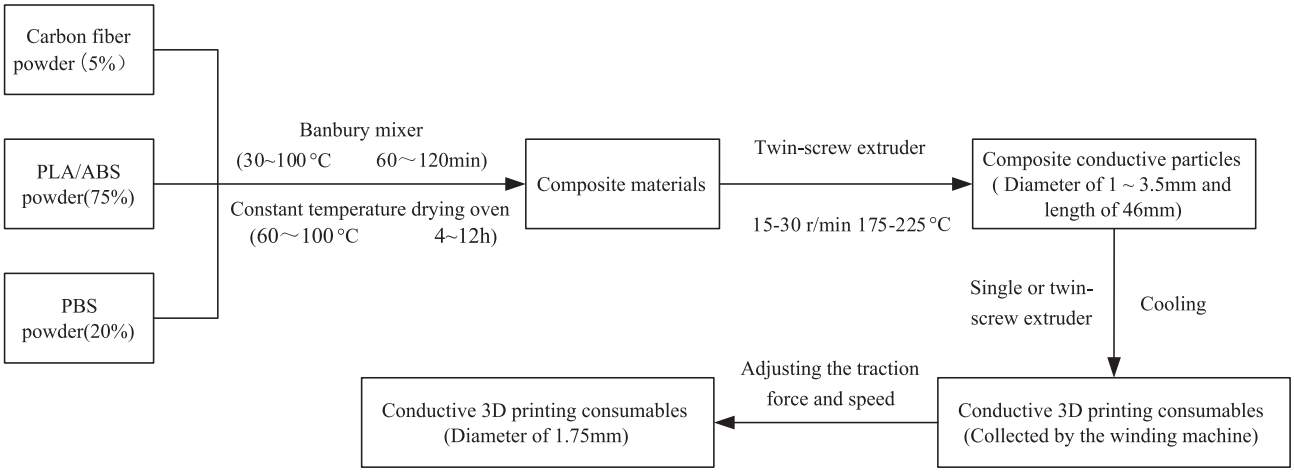

Fig. 1. Making flow chart of conductive 3D printing consumable.

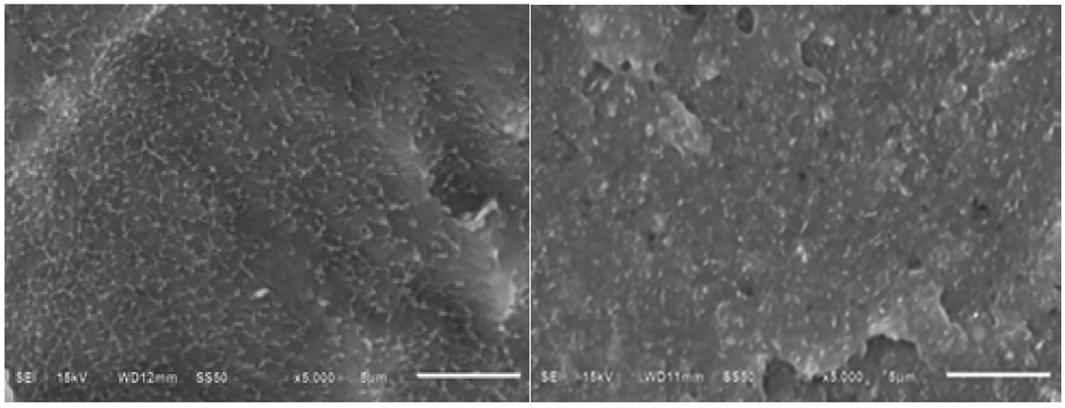

Fig. 2. The SEM images of conductive ABS and PLA.

specimen were recorded simultaneously in each set of experiments.

3.1. Preliminary experiment

3.1.1. Influences of different materials on the performance of the specimen

3.1.1.1. Specimen preparation. Geobelt specimens were printed with P and A as the shells and CP and CA as conducting wires. In the process of printing, it was found that ABS material had serious problems of warping edges and them are not suitable for experiments. Therefore, when material A is selected as the shell printing material, only CP material is selected as the conductive wire for manufacturing. The shape of the conductive wire is shown below with a diameter of 2 mm. The tensile tests were carried out in general conformance with the ASTM D6637 test protocol. However, due to the difference between the sensing geobelt and the ordinary plastic geogrid in some properties, the specimens preparation process has been adjusted accordingly. The size of the specimen is 120*12*3 mm (Fig. 3). The effective range of the specimen is 30 mm, and each supporting end is 45 mm. Print 3 samples of each kind material. Weld conductive metal wires at both ends of the test piece. The resistance is measured as the initial resistance.

3.1.1.2. Tensile strength test. In this experiment, different types of geobelt specimens were stretched at room temperature to explore the influence of different material types on the mechanical properties of finished geobelt products. Put 9 specimens into the universal testing machine, and clamp the specimens to ensure that the longitudinal axis of the specimens coincides with the center line of the upper and lower clamps. The clamping force of the specimen should be appropriate to prevent the specimen from slipping out of the clamping device. (As shown in Fig. 4.)

According to the provisions of the ASTM D6637 test protocol on geotextile grid experiment, the tensile rate is 20%/min of the effective range. In order to make the process of resistance change easier to observe, the tensile speed of 5 mm/min is chosen to carry out the test until the specimen is destroyed. The tensile test specimen is composed of 3 specimens with the same material. The change of resistance is recorded by universal electric meter, and the law of relative change rate of resistance of three groups specimens during loading is analyzed with the increase of tension.

3.1.1.3. Experimental results analysis. Based on the above three groups of experiments, the experimental results of the resistance of geobelt specimens with tension are obtained (As shown in the Tables 2–4).

Firstly, the final results of the above experiments are compared from the tensile strength. The tensile strength of PLA or ABS material was 50.94 MPa and 30.33 MPa, respectively. The tensile strength of PLA and ABS material was reduced after adding conductive material. Therefore, the tensile strength of the specimens made of A-CP material is relatively low, while that of the specimens made of PLA material is relatively high.

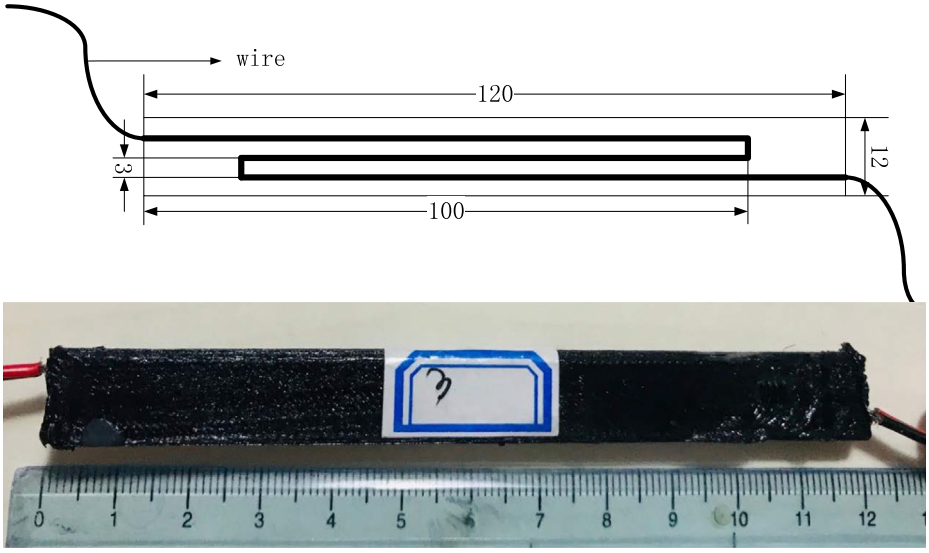

Fig. 3. Schematic diagram of specimen specifications.

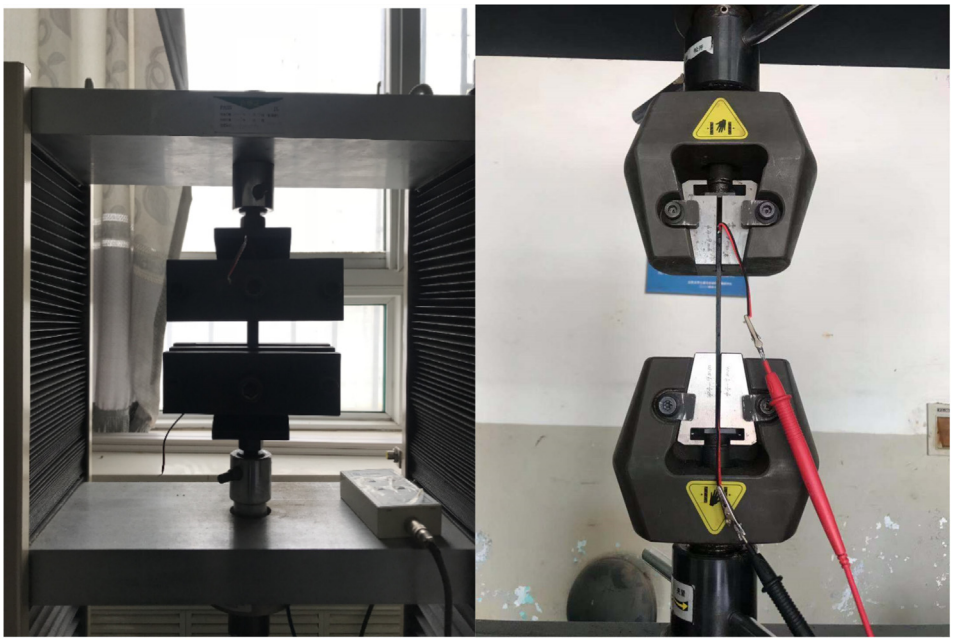

Fig. 4. Tensile strength test.

Table 2
Experimental results of P-CP material specimens.

NO.	Initial resistance (MΩ)	Final resistance (MΩ)	Rate of resistance change (%)	Elongation at failure (%)	Tensile strength (MPa)
1	0.053	0.092	74.9	9.62	43.3
2	0.050	0.076	50.3	8.73	35.3
3	0.068	0.076	12.4	8.20	30.3

Table 3
Experimental results of P-CA material specimens.

NO.	Initial resistance (MΩ)	Final resistance (MΩ)	Rate of resistance change (%)	Elongation at failure (%)	Tensile strength (MPa)
1	0.372	0.645	73.4	10.48	49.5
2	0.256	0.476	85.9	11.01	50.5
3	0.322	0.523	62.4	9.19	41.5

Table 4
Experimental results of A-CP material specimens.

NO.	Initial resistance (MΩ)	Final resistance (MΩ)	Rate of resistance change (%)	Elongation at failure (%)	Tensile strength (MPa)
1	0.023	0.030	28.8	8.13	25.5
2	0.027	0.033	24.2	7.97	25.2
3	0.016	0.025	52.2	9.12	25

Table 5
Experimental group with liner conductive wire built in.

NO.	Initial resistance (MΩ)	Final resistance (MΩ)	Rate of resistance change (%)	Elongation at failure (%)	Tensile strength (MPa)
1	0.352	0.401	14.1	10.50	51.7
2	0.478	0.541	13.9	10.90	54.2
3	0.382	0.410	7.1	9.43	53.2

From the perspective of resistance variation range, the resistance variation rates of P-CP group are 12.4%, 50.3% and 74.9% respectively, which are very unstable. This is because the conductive material and the non-conductive shell are the same base material, which are easy to be mixed together in the process of 3D printing, resulting in that the resistance value is affected by the shell material. The resistance variation rate of P-CA was between 60% and 90%, and that of the A-CP group was between 20% and 55%.

From the perspective of average elongation, the average elongation of specimens in the P-CA group at failure was 8.85%, that in the A-CP group was 10.23%, and that in the A-CP group was 7.41%.

The experimental process is analyzed as follows. The resistance value R at each time is subtracted from the initial resistance R_0 to obtain the resistance change value R_Δ. The maximum resistance change value Rm of the specimen is 1. The normalized resistance value r is obtained by dividing the resistance change value R_Δ by the resistance change maximum Rm. The peak force Fm of the specimen is 1, and the normalized tensile force f is obtained by dividing the tensile force F of the specimen by the peak force Fm.

$$R_\Delta = R - R_0 \tag{3-1}$$

$$\mathrm{r} = \frac{R_\Delta}{R_m} \tag{3-2}$$

$$\mathrm{f} = \frac{F}{F_m} \tag{3-3}$$

The resistance and tension values in the process of experiment are normalized as ordinates. The ultimate strain is the strain after each test specimen is damaged by tension. The ultimate strain is recorded as $\varepsilon_{ult} = 1$. With the strain as the abscissa, the following results are obtained from the above three groups of experiments. (see Fig. 5).

Among them, black represents No. 1 in each group, blue represents No. 2, and red represents No. 3. As can be seen from the above results, the resistance changes of the specimens with P-CP and P-CA are more regular than those of the A-CP group, and reflect the stress changes better, while the resistance changes of the A-CP group are more irregular. As can be seen from the figure above, when the strain reaches 50%ε_{ult}, the resistance of the P-CP group begins to change. A-CP group began to change after the strain reached 30%εult. That is to say, the resistance of A-CP group specimens can show the change of stress under smaller strain, which is sensitive to the change.

Based on the above considerations, P-CA material is selected for specimen production.

3.1.2. The influence of the layout of conductive wire on the properties of specimen

3.1.2.1. Influence of longitudinal and transverse layout of conducting wire. P-CA material is used to print geobelt specimens according to the two paths of conductive wire layout shown in Fig. 6. The specimens are in accordance with the previous experiment. 3 specimens were printed for each pattern. Conductive metal wires are welded at both ends of the specimens. Resistance is measured and recorded as initial resistance. The specimens were put into a universal testing machine for tensile test. The tensile speed was 5 mm/min, and resistance changes and tensile values of the specimen were recorded.

The following results (Table 5 and Table 6) were obtained through experiments.

Comparing the experimental results of geobelt specimens formed with linear conductive wire and folded transverse conductive wire, it is found that the distribution of transverse internal conductive wire will reduce the tensile strength of geobelt. This is because the layout direction of the internal transverse wire is perpendicular to the direction of the tension, which makes the specimen easier to break under the action of the tension, the fracture surface of the specimen is just in the position of the transverse conductive wire when it is damaged. Moreover, the layout of conductive wires greatly reduces the elongation of specimens, which results in relatively more brittle failure. Therefore, the orientation of conductive wire should be the same as the direction of tension.

From the response of resistance to the change of tension, the change rate of resistance is very small when liner conductive wire is built in. That is to say, its sensitivity to tension is low. Compared with the results of experimental group 2 in Table 3, it is found that it is necessary to increase the number of longitudinal conducting wires.

Fig. 7 shows the variation law of normalized resistance and normalized tension with strain. It can also be seen from the above results that the maximum strain of the specimens with folded

Table 6
Experimental group with folded transverse conductive wires built in.

NO.	Initial resistance (MΩ)	Final resistance (MΩ)	Rate of resistance change (%)	Elongation at failure (%)	Tensile strength (MPa)
1	0.390	0.425	8.9	3.70	29.2
2	0.439	0.543	23.7	3.63	29.2
3	0.347	0.380	9.5	4.23	27.8

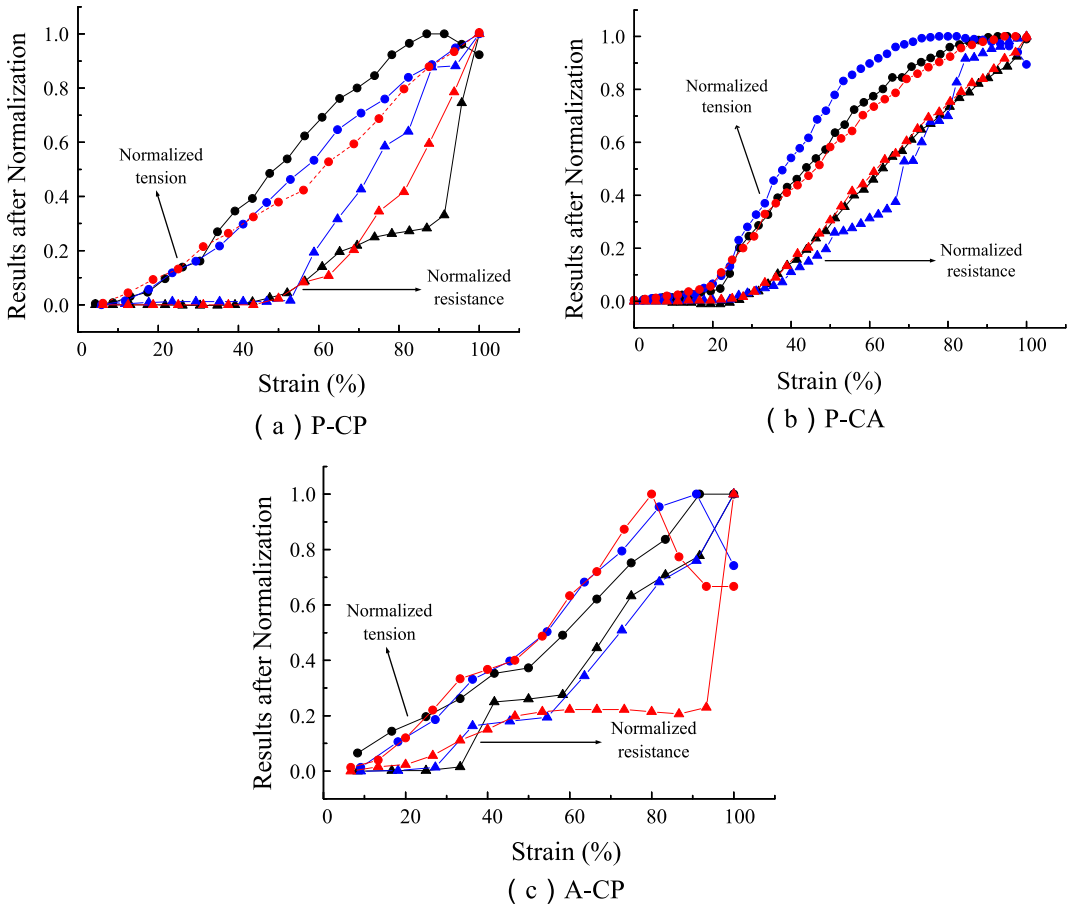

Fig. 5. The normalized resistance and normalized tensile value change with strain for different materials.

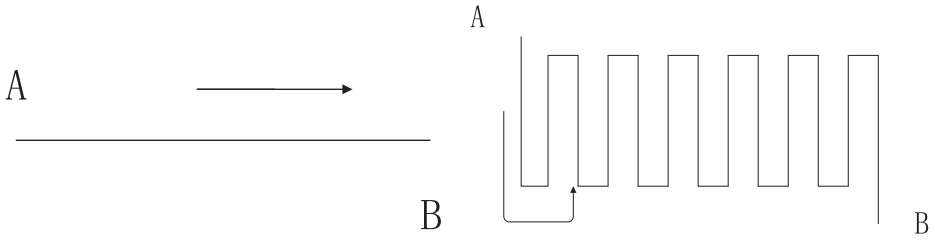

Fig. 6. Printing path diagram of conducting wire.

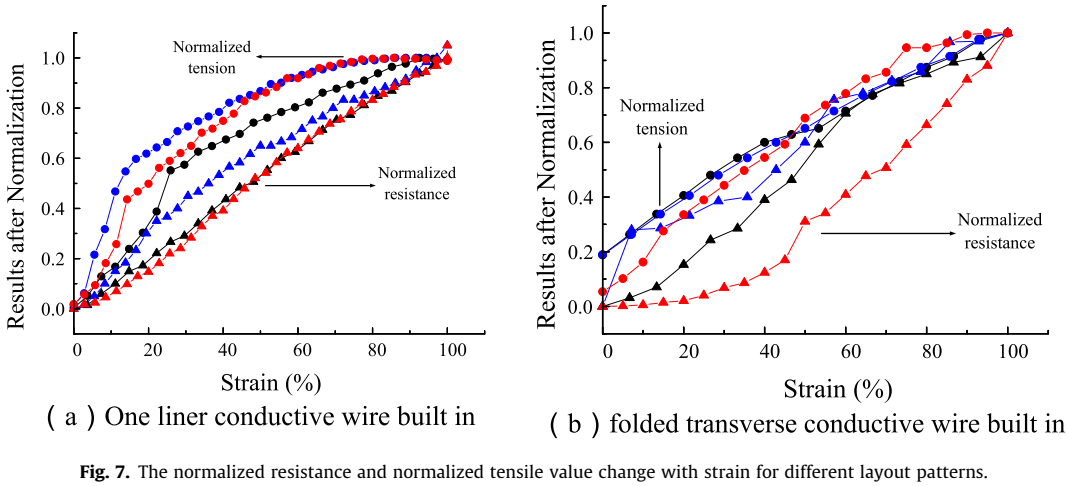

Fig. 7. The normalized resistance and normalized tensile value change with strain for different layout patterns.

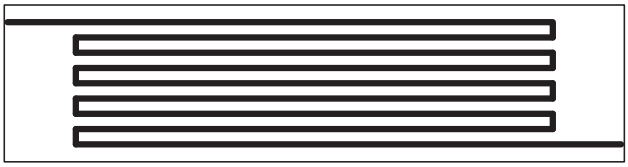

Fig. 8. Schematic diagram of layout of conductive wire inside the specimen.

transverse conductive wires inside is smaller, and the effect of the change of resistance with strain on the tension is not good.

Therefore, the longitudinal resistance wire layout was selected for the following sample production.

3.1.2.2. Influence of the number of longitudinal conductive wires. In order to observe the relationship between the number of built-in longitudinal conductive wires and the variation of resistance, the following experiments were carried out.

Table 7
Experimental results of different number of longitudinal conducting wires.

Number of Conductive wires	Initial resistance (MΩ)	Final resistance (MΩ)	Rate of resistance change (%)	Elongation at failure (%)	Tensile strength (MPa)
1	0.315	0.506	60.6	9.64	35
3	0.345	0.585	69.6	9.56	34.8
5	0.395	0.694	75.7	9.44	34
7	0.452	0.799	76.8	9.26	33.5
9	0.611	1.342	119.6	9.02	32.9

Table 8
Tensile test results of specimens under slow loading.

NO.	Initial resistance (MΩ)	Final resistance (MΩ)	Rate of resistance change (%)	Elongation (%)	Tensile stress (MPa)
1	0.135	0.157	16.8	6.16	41
2	0.137	0.157	14.7	5.56	42.3
3	0.152	0.173	14.2	7.54	45

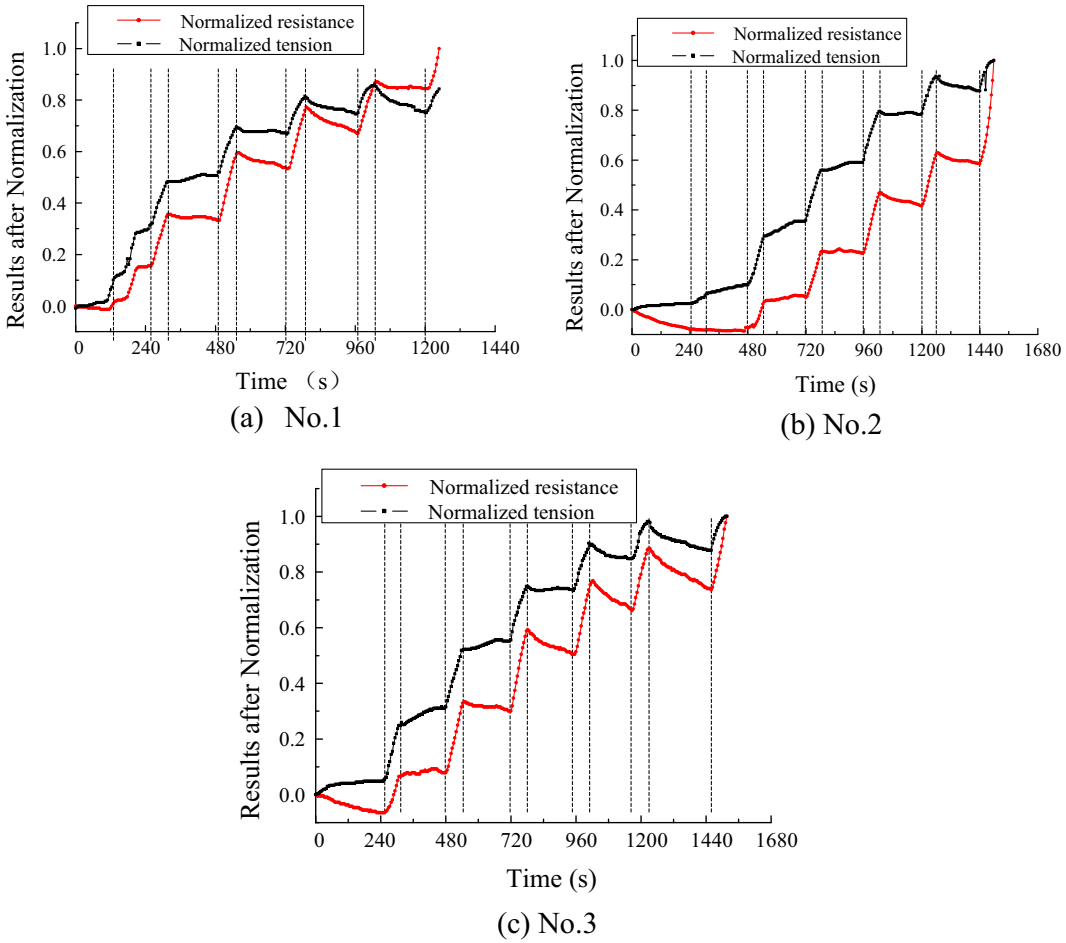

Fig. 9. Normalized resistance and normalized stress under slow loading.

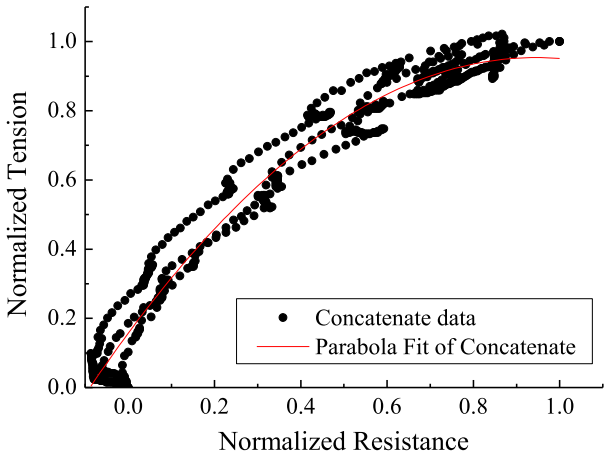

Fig. 10. The relationship between resistance change and stress change.

Print the geobelt specimen with a length of 100 mm, a width of 21 mm and a thickness of 3 mm, and use P-CA material to arrange 1, 3, 5, 7, 9 longitudinal and uninterrupted conductive wires (as shown in the Fig. 8). A tensile test was carried out with these specimens. The tensile speed was set at 5 mm/min until the specimen was destabilized and destroyed. At the same time, the changes of tension and resistance of the specimen were recorded, and the following data were obtained.

It is found from the above table that when the number of longitudinal conducting wires increases, the initial resistance of the specimen gradually increases. This is because the resistance increases as the length of the internal conducting wire increases.

The values of rate of resistance change in Table 7 are equal to the gauge factors. It is found from the Table 7 that when the number of longitudinal conducting wires increases, the gauge factor increases. When the longitudinal conductive wire increases from 1 to 9, the gauge factor increases from 0.6 to 1.2. Compared with other published composites (gauge factors between 1 and 10) [36], the developed self-sensing composites are less sensitive to load. This probably can be explained as that the majority part of the belt is made by nonconductive plastic. A larger gauge factor value can be obtained by increasing the number of conducting wires.

It is also found that the tensile strength of the specimen has a tendency to decrease. However, the tensile strength does not decrease to a large extent when the longitudinal conductive wire increases from 1 to 9. With the increase of the number of longitudinal conducting wires, the final resistance of the specimen gradually increased, and the growth rate of the resistance at the end of the experiment was also gradually increased. This is because when the specimen is deformed under tension, the more the number of longitudinal conductor wires arranged inside, the more the length of the conductor wires will be amplified, and the more the resistance will be changed.

Therefore, when selecting the number of longitudinal conducting wires, it is necessary to consider both increasing the number of conducting wires will reduce the tensile strength of the specimen, and increasing the number of conducting wires can amplify the change of resistance.

3.2. The influence of slow loading on the tensile strength and resistance of specimens

3.2.1. Specimens preparation and experimental process

In real engineering cases, the external forces may act slowly and non-uniformly on the geobelts. In order to study the changes of stress and tensoresistivity of self-monitoring polymer geobelts under slow loading external forces, a set of tests was designed. Three specimens of 120 mm × 12 mm × 3 mm were made of P-CA material. The internal conductive wires are arranged longitudinally in three strips. After specimens are firmly clamped in the testing machine, the specimens are stretched for 1 min at a stretching speed of 0.2 mm/min, and then the constant strain state is simulated at a stretching speed of 0.03 mm/min, which is maintained for 3 min. This geobelt tension test is carried out repeatedly until the specimen is broken. The purpose of this loading method is to apply a relatively slow loading speed to the specimen, simulate the practical application conditions, and at the same time, reduce the testing time to the greatest extent.

Table 9
Experimental case table.

Phases	Tensile speed (% ε_{max} / min)	Final strain ε_f (% ε_{max})	Cycle times
1	10	10	10
2	10	50	5
3	25	25	5
4	25	50	5
5	50	25	5
6	50	50	5

3.2.2. The tendency of normalized resistance and normalized tension in the process of tensile failure

During the tests, we found that once the tensile strength of the specimen is reached, its internal conductive circuit will be seriously damaged, the change of resistance fluctuates obviously, therefore, only the data of resistance and strain before specimens reaches the tensile strength are analyzed, and the results in Table 8 are obtained.

It can be seen that under slow loading, the elongation of the three specimens with the effective range of 30 mm near failure is 6.16%, 5.56% and 7.54% respectively. Compared with one thousandth elongation of optical fiber, the monitoring range of self-monitoring polymer geobelts is larger. Especially in the engineering practice of earth structures, the deformation is often large, so this geobelt can play its advantages. It is observed that the tension and resistance in tension test vary with the change of the tension rate and form several matching stages.

The normalized tension and normalized resistance are plotted in Fig. 9.

From the results of Fig. 9, it can be seen that with the increase of time, the tensile stress of the specimens increases gradually. Comparing the three groups of experimental results, it is found that the tensile strength of the specimens is basically the same, all around 40 MPa. At the loading rate of 0.2 mm/min, the tensile stress increases gradually and the resistance increases slightly. At the loading rate of 0.03 mm/min, the stress in the specimen decreases gradually. This is because when the specimen is subjected to external forces, a continuous deformation occurs, during which the load of the specimen keeps increasing. However, when the increase of external force is greatly reduced, the specimen will no longer undergo obvious rapid deformation. On the contrary, because of stress relaxation, the stress begins to decline. At this time, it can be seen from the curve that the resistance is almost unchanged or slightly decreased, which is consistent with the trend of the tension of the specimen. When the specimen reaches the tensile strength, the resistance begins to rise significantly until the specimen is pulled off and the resistance has no changes.

The normalized tension and normalized resistance are plotted in Fig. 10. As shown in the figure, the changes of resistance of the geobelt specimen can reflect the changes of its tension. The relationship between the two can be fitted with the following quadratic polynomial function,

$$f = A + Br + Cr^2 \quad (3\text{-}4)$$

where r is the normalized resistance, f is the normalized tension, A, B and C are fitted parameters. Fig. 10 shows the fitted result of three groups of tests. The fitting parameters A = 0.157, B = 1.686, C = −0.892. A represents the intercept of a parabola. When the resistance changes to zero and starts to rise, the geobelt has been subjected to a certain tension. This means that the resistance begins to increase when the tension reaches a certain value, which is in agreement with the experimental results.

When the specimen reaches the tensile strength, it will lose its stability, then it reaches the subsequent failure, and the resistance of the specimen increases rapidly to its peak value, at the same time.

In the real cases, the stage of tension can be deduced by normalized resistance value. In engineering practice, the preliminary experiments should be carried out before the geobelts are come into service to find the initial, the maximum resistance and tensile stress in the vicinity of failure of the geobelts because of the influence of geobelts specifications on the initial resistance. The resistance value at a certain time was measured during the actual measurement. Formulas (3-1), (3-2) are used to obtain the normalized resistance value r, then formula (3-4) is used to obtain the normalized tension value f, and finally formula (3-3) is used to calculate the tension of geobelt at this time.

3.3. Study on the repeatability of self-monitoring polymer geobelts

3.3.1. Specimens preparation and experimental process

In order to investigate the self-sensing characteristics and repeatability of sensing samples, the following experiments were carried out.

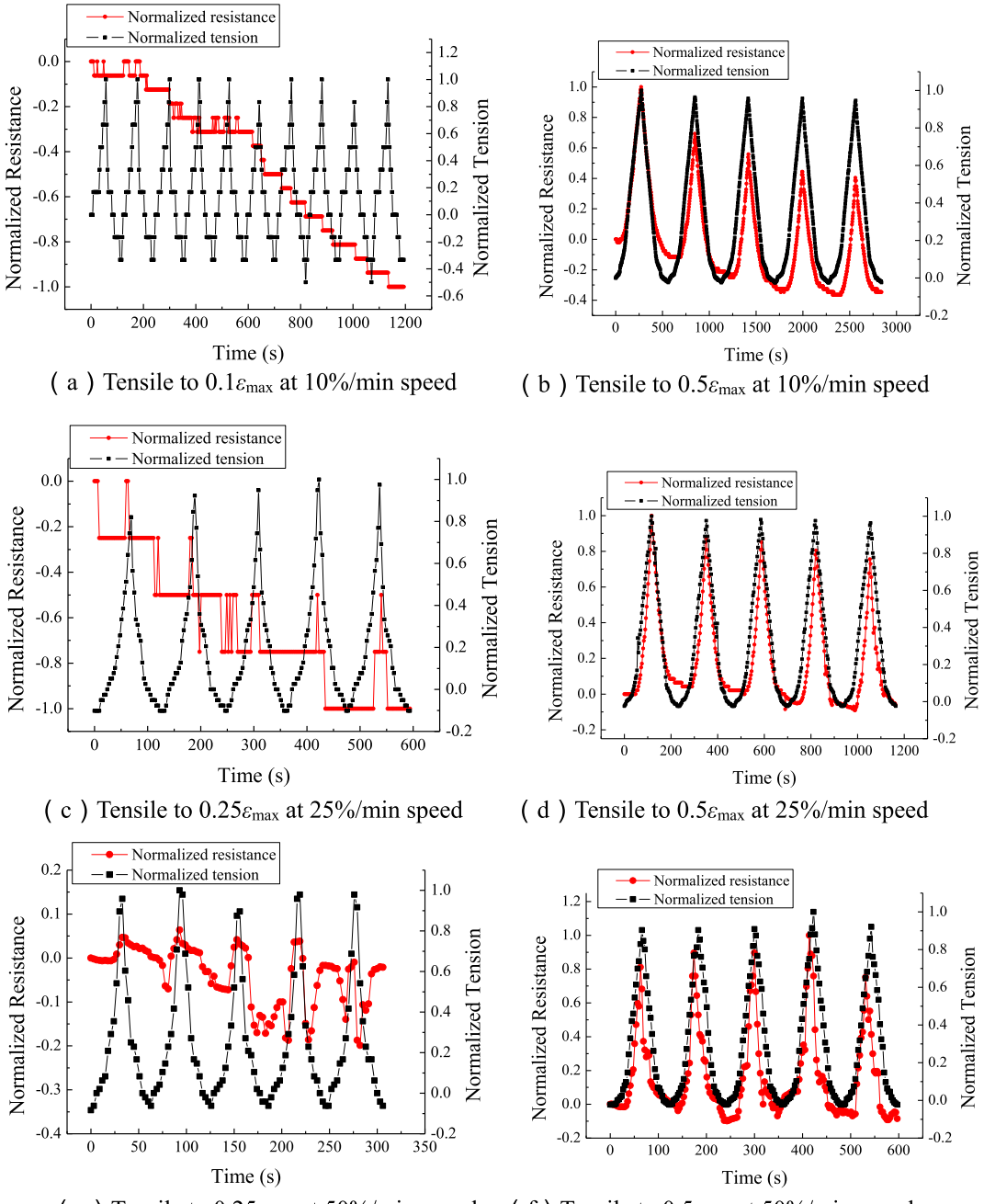

Fig. 11. Experimental results under cyclic load.

One specimen was used to carry out this study, and it was made of P-CA material, and a conductive wire with longitudinal folded for three times was arranged inside, the size of which was 120 mm × 12 mm × 3 mm. From the experiments in the 3.1, it can be seen that the ε_{ult} of the specimens is about 10%. In order to keep the specimens from being pulled off under cyclic load, the maximum strain is 7%, which is recorded as ε_{max} = 7%. After specimen was firmly clamped in the testing machine, loading and unloading are carried out according to the tensile speed of 10% ε_{max}/min, 25% ε_{max}/min and 50% ε_{max}/min, respectively. Six loading and unloading cycles are carried out. The specific tensile speed and fanal strain are shown in the Table 9. The purpose of this loading method is to simulate the tension and compression of the specimens in engineering practice, to investigate whether the specimens fail under such repeating tension and compression loadings, and the effect of strain speed and final strain on the tensoresistivity of specimens. At the same time, in order to make all the resistance values collected by the experiment under cyclic load effective, the maximum value of the final strain ε_f of the experiment is chosen to be 50% ε_{max}.

3.3.2. The variation trend of normalized resistance and normalized tension under cyclic load

The normalized resistance and the normalized tension change with time are plotted in a graph. The results of the above six groups of experiments are shown in Fig. 11.

As shown in Fig. 11 (a), 10 times of cyclic loading were applied to a specimen at 10% ε_{max}/min tension speed. The maximum strain of each cycle was 0.1 ε_{max}. However, it is found that the resistance did not changed periodically with the change of strain but present step-like decrease. This is may be caused by the conductive lines inside the specimen are folded and arranged. Under slight strain, the carbon fiber powder of the conductive network at the turning point has more chances to contact with each other. After 10 cycles, the resistance decreases by 1.29%. After that, the specimen is stretched to 0.5 ε_{max} at the same tensile speed. After 5 cycles, as shown in Fig. 11 (b) that the resistance change corresponding to the tension can be obtained by increasing the maximum strain of the specimen at the same tensile speed, but the resistance decreased mildly when the strain is zero at the end of each cycle.

Then, the specimen is subjected to 5 cycles of cyclic loading at 25% ε_{max}/min tensile speed. The maximum strain of each cycle is 0.25 ε_{max}. It can be found that the resistance has a step-like decrease with tiny peaks when the tension reaches the peak value (As shown in Fig. 11 (c)). It shows that the strain at this time is not enough to make the resistance change to reflect the cyclic loading. At the end of the third phase, the resistance decreases by 1.10%. Then the specimen is stretched to 0.5 ε_{max} at the same tensile speed. After 5 cycles, it can be seen that the change of resistance fits well with the change of the cyclic loading. (As shown in Fig. 11 (d)).

Finally, the specimen is subjected to the loading at the tensile speed of 50% ε_{max}/min. The maximum strains of each cycle are 0.25 ε_{max} and 0.5 ε_{max}, respectively. The results are shown in Fig. 11 (e) and Fig. 11 (f). It can be seen that when the final strain reaches 0.25 ε_{max} at the speed of 50% ε_{max}/min, the change of resistance begins to reflect the change of tension roughly. When the final strain increases to 0.5ε_{max}, the change of resistance can reflect well with the cyclic loading. By comparing Fig. 11 (b), (d) and (f), it can be seen that when the strain is large enough, the change of resistance can reflect the change of tension. However, too small or too large the tensile speed has a slight effect on the results.

In order to find the minimum strain which can cause the change of the resistance of the specimen, the experimental data of 2, 3, 4th phases without normalization are plotted as Fig. 12. By observing the data of the experimental process, in the 2nd phase, the initial tension when the resistance start to reflect the loading is gradually decreasing. That is to say, with increase of number of cyclic loading, the sensitivity gradually increases. In the 3rd phase, the tension of the specimen has not reached the lowest value which can trigger the feedback of resistance, so the change of resistance is not obvious. In the 4th phase, the lowest value of the tension which causes the resistance change tends to be stable, which is around 300 N, and the corresponding strain is 0.3 ε_{max}. So the test range of the specimens is above 0.3 ε_{max} i.e. 2.1% ε_{ult}.

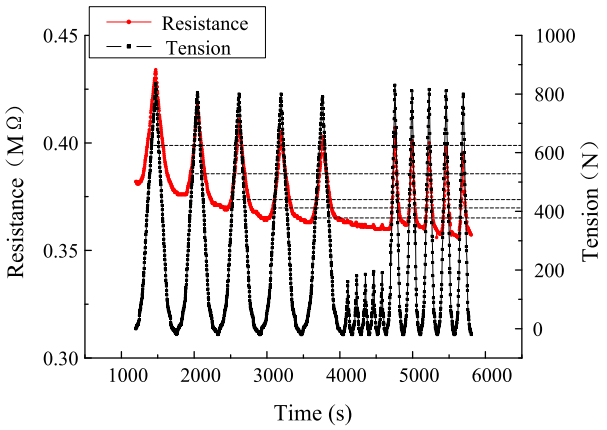

Fig. 12. The resistance and tension of the specimen in the 2, 3, 4th phases.

4. Conclusion

In this study, a series of tests were performed to study the development and laboratory evaluation of a self-monitoring Geobelts. Based on the test results, a preliminary model was proposed to monitoring soil deformation. The tensoresistivity performance of self-monitoring Geobelts made by 3D printing after loading has been evaluated.

The following conclusions were drawn as follows:

1. PLA material is chosen as the base material and conductive ABS material as the internal conductive wire for the geobelt. The orientation of conductive wire should be consistent with the direction of tension.
2. The increase of the number of conductive wire layout will reduce the tensile strength of geobelts to some extent, but the resistance change rate under the action of tension or pressure will be greatly increased, which reflects the strain more accurately. Therefore, the number of longitudinal conductive wires can be increased appropriately when the width and size of the geogrid are allowed.
3. The relationship between resistance and stress at both ends of the grid can be fitted by parabola. The fitting result is $f = A + Br + Cr^2$.
4. In the process of loading, the normalized resistance of specimens increases with the increase of tension, while in the process of unloading, the normalized resistance decreases with the decrease of tension. After several cycles, the specimens still retain such characteristics, showing good self-perception and repeatability.
5. Based on experimental data, the test range of this 3D printing geobelt is 2.1–10% of effective length.

5. The Data Availability Statement

Some or all data, models, or code that support the findings of this study are available from the corresponding author upon reasonable request.

CRediT authorship contribution statement

Jiong Zhang: Conceptualization, Methodology, Writing - review & editing. **Rui She:** Methodology, Data curation, Writing - original draft. **Shuang Xia:** Validation, Data curation. **Zhaoxia Dai:** Resources. **Nian Hu:** Resources. **Xinzhuang Cui:** Data curation. **Ruonan Han:** Data curation. **Ruiping Ming:** Data curation. **Guodong Ma:** Data curation.

Declaration of Competing Interest

The authors declare that they have no known competing financial interests or personal relationships that could have appeared to influence the work reported in this paper.

Acknowledgements

The authors would like to thank the National Key Research and Development Project (2018YFB1600100), Natural Science Foundations of Shandong Province, China (ZR2018MEE046) and the Fundamental Research Funds for the Central Universities (No. 2018JC040).

References

[1] K.S.C. Kuang, C.Y. Tan, S.H. Chew, S.T. Quek, Monitoring of large strains in submerged geotextile tubes using plastic optical fibre sensors, Sens. Actuators, A 167 (2) (2011) 338–346.
[2] R.K. Rowe, C.T. Gnanendran, Geotextile strain in a full scale reinforced test embankment, Geotext. Geomembr. 13 (12) (1994) 781–806.
[3] R.K. Rowe, B.L.J. Mylleville, A geogrid reinforced embankment on peat over organic silt: a case history, Can. Geotech. J. 33 (1) (1996) 106–122.
[4] C.T. Gnanendran, A.P.S. Selvadurai, Strain measurement and interpretation of stabilising force in geogrid reinforced, Geotext. Geomembr. 19 (3) (2001) 177–194.
[5] B.V.S. Viswanadham, D. Konig, Studies on scaling and instrumentation of a geogrid, Geotext. Geomembr. 22 (5) (2004) 307–328.
[6] Z.F. Wang, J. Wang, Q.M. Sui, X.M. Liang, L. Jia, S.C. Li, et al., Development and application of smart geogrid embedded with fiber bragg grating sensors, J. Sens. 2015 (2015) 1–10.
[7] M. Silva-Lopez, A. Fender, W.N. Macpherson, et al., Strain and temperature sensitivity of a singlemode polymer optical fibre, Opt. Lett. 30 (2005) 3129–3131.
[8] P. Lenke, S. Liehr, K. Krebber, F. Weigand, E. Thiele, Distributed strain measurement with polymer optical fiber integrated in technical textiles using the optical time domain reflectometry technique, in: Proceedings of the 16th International Conference on Plastic Optical Fibre, 2007, pp. 21–24.
[9] I.R. Husdi, K. Nakamura, S. Ueha, Sensing characteristics of plastic optical fibres measured by optical time-domain reflectometry, Meas. Sci. Technol. 15 (2004) 1553–1559.
[10] A. Appajaiah, Climatic stability of polymer optical fibers, BAM Dissertation Series, vol. 9, http://www.bam.de/en/service/publikationen/publikationen medien/dissertationen/diss 9e vt.pdf.
[11] R. Kusy, Chapter 1: applications, in: S.K. Bhattacharya (Ed.), Metal-filled Polymers: Properties and Applications, CRC Press, 1986.
[12] X.Z. Cui, S.Q. Cui, T. Lu, L. Zhang, Y.L. Wang, J. Li, Evaluation of the performance of sensor-enabled geobelts after cyclic loading, Constr. Build. Mater. 185 (2018) (2018) 414–422.
[13] X.Z. Cui, Q. Jin, S.Q. Cui, Y.L. Wang, L. Zhang, Z.X. Wang, Laboratory tests on the engineering properties of sensor-enabled geobelts (SEGB), Geotext. Geomembr. 46 (1) (2018) 66–76.
[14] J. Li, X.Z. Cui, Q. Jin, J.W. Su, S.Q. Cui, Y.L. Wang, Laboratory investigation of the durability of a new smart geosynthetic material, Constr. Build. Mater. 169 (2018) 28–33.
[15] M. Knite, V. Teteris, A. Kiploka, I. Klemenoks, Reversible tensoresistance and piezo-resistance effects in conductive polymer-carbon nanocomposites, Adv. Eng. Mater. 6 (9) (2004) 742–746, https://doi.org/10.1002/adem.200400062.
[16] M.H. Al-Saleh, U. Sundararaj, Electromagnetic interference (EMI) shielding effectiveness of PP/PS polymer blends containing high structure carbon black, Macromol. Mater. Eng. 293 (7) (2008) 621–630, https://doi.org/10.1002/mame.200800060.
[17] C. Lin, D.D.L. Chung, Graphite nanoplatelet pastes vs. carbon black pastes as thermal interface materials, Carbon 47 (1) (2009) 295–305, https://doi.org/10.1016/j.carbon.2008.10.011.
[18] K. Hatami, R.J. Bathurst, Development and verification of a numerical model for the analysis of geosynthetic reinforced-soil segmental walls under working stress conditions, Can. Geotech. J. 42 (4) (2005) 1066–1085.
[19] K. Hatami, R.J. Bathurst, Numerical model for reinforced soil segmental walls under surcharge loading, ASCE J. Geotech. Geoenviron. Eng. 132 (6) (2006) 673–684.
[20] K. Hatami, B.P. Grady, M.C. Ulmer, Sensor-Enabled Geosynthetics: use of conducting carbon networks as geosynthetics sensors, ASCE J. Geotech. Geoenviron. Eng. 135 (7) (2009) 863–874.
[21] H. Yazdani, K. Hatami, E. Khosravi, K. Harper, B.P. Grady, Strain-sensitive conductivity of carbon black-filled pvc composites subjected to cyclic loading, Carbon 79 (2014) 393–405.
[22] B.E. Smith, H. Yazdani, K. Hatami, Three-dimensional imaging and quantitative analysis of dispersion and mechanical failure in filled nanocomposites, Compos. A Appl. Sci. Manuf. 79 (2015) 23–29.
[23] Hessam Yazdani, Kianoosh Hatami, Sensor-enabled geogrids for stabilization and performance monitoring of earth structures: state of development, Int. J. Geosynth. Ground Eng. 2 (4) (2016), https://doi.org/10.1007/s40891-016-0077-z.
[24] H. Yazdani, B.E. Smith, K. Hatami, Electrical conductivity and mechanical performance of multiwalled CNT-filled polyvinyl chloride composites subjected to tensile load, Appl. Polym. Sci. 133 (29) (2016), https://doi.org/10.1002/APP.43665.
[25] H. Yazdani, B.E. Smith, K. Hatami, Multi-walled carbon nanotube-filled polyvinyl chloride composites: influence of processing method on dispersion quality, electrical conductivity and mechanical properties, Compos. A Appl. Sci. Manuf. 82 (2016) 65–77.
[26] H. Yazdani, B.E. Smith, K. Hatami, Multiscale 3D dispersion characterization of carbon nanotube-filled polymer composites using microscopic imaging and data mining, in: W.I. Milne, M. Cole, S. Mitura (Eds.), Carbon Nanotechnology, One Central Press, Manchester, UK, 2016, pp. 135–158 (Chapter 6). http://www.onecentralpress.com/carbon-nanotechnology/.
[27] H. Yazdani, K. Hatami, B.P. Grady, Sensor-enabled geogrids for performance monitoring of reinforced soil structures, ASTM J. Test. Eval. 44 (01) (2016) 391–401.
[28] K. Hatami, B.P. Grady, M.C. Ulmer, Sensor-enabled geosynthetics: use of conducting carbon networks as geosynthetic sensors, J. Geotechn. Geoenviron. Eng. 135 (7) (2009) 863–874, https://doi.org/10.1061/(ASCE)GT.1943-5606.0000062.
[29] K. Hatami, B. Grady, M. Ulmer, Closure to 'sensor-enabled geosynthetics: use of conducting carbon networks as geosynthetic sensors' by Kianoosh Hatami, Brian P. Grady, and Matthew C. Ulmer. J. Geotechn. Geoenviron. Eng. 37(4) (2011) 435–436. http://dx.doi.org/10.1061/(ASCE)GT.1943- 5606.0000472.
[30] A. Fathi, K. Hatami, B.P. Grady, Effect of carbon black structure on low-strain conductivity of polypropylene and low-density polyethylene composites, Polym. Eng. Sci. 52 (3) (2012) 549–556, https://doi.org/10.1002/pen.22115.
[31] K. Hatami, A. Hassanikhah, H. Yazdani, B. Grady, Tensoresistive PVC coating for sensor-enabled geogrids, J. Nanomech. Micromech. (2013), https://doi.org/10.1061/(ASCE)NM.2153- 5477.0000070, A4013016.
[32] H. Yazdani, K. Hatami, T. Hawa, B.P. Grady, Molecular dynamics simulation of sensor-enabled geosynthetics, in: Nanotechnology, Nano Science and Technology Institute, Santa Clara, US, 2012, pp. 673–676.
[33] H. Yazdani, K. Hatami, T. Hawa, B.P. Grady, 'Atomic-scale simulation of sensor-enabled geosynthetics for health-monitoring of reinforced soil slopes and embankments, in: Geo-Congress 2013: Stability and Performance of Slopes and Embankments III, American Society of Civil Engineers, 2013, pp. 1522–1528. doi: http://dx.doi.org/10.1061/9780784412787.152.
[34] A. D'Alessandro, M. Rallini, F. Ubertini, et al., Investigations on scalable fabrication procedures for self-sensing carbon nanotube cement-matrix composites for SHM applications, Cem. Concr. Compos. 65 (2016) 200–213.
[35] Francis Avilés, Andrés I Oliva-Avilés, Cen-Puc M. Piezoresistivity, Strain and damage self-sensing of polymer composites filled with carbon nanostructures, Adv. Eng. Mater. (2018) 1701159.
[36] A. Poudel, N. Karode, P. Mcgorry, et al., Processing of nanocomposites using supercritical fluid assisted extrusion for stress/strain sensing applications, Compos. B Eng. 165 (2019) 397–405.